






Quantum compressed sensing-based compound system for ranging/vibration measurement

HONGQI NIU,^{1,2} LIU YANG,^{1,2} JIANYONG HU,^{1,2,3,*} CHANGGANG YANG,^{1,2} GUOSHENG FENG,⁴ ZHIXING QIAO,⁴  RUIYUN CHEN,^{1,2}  CHENGBING QIN,^{1,2}  GUOFENG ZHANG,^{1,2} LIANTUAN XIAO,^{1,2,3} AND SUOTANG JIA^{1,2}

¹State Key Laboratory of Quantum Optics and Quantum Optics Devices, Institute of Laser Spectroscopy, Shanxi University, Taiyuan 030006, China

²Collaborative Innovation Center of Extreme Optics, Shanxi University, Taiyuan 030006, China

³College of Physics, Taiyuan University of Technology, Taiyuan 030600, China

⁴College of Medical Imaging, Shanxi Medical University, Taiyuan 030001, China

*jyhu@sxu.edu.cn

Received 15 May 2024; revised 13 August 2024; accepted 5 September 2024; posted 6 September 2024; published 24 September 2024

Frequency-modulated continuous-wave (FMCW) lidar offers high precision and strong interference resistance, capable of synchronously measuring target motion speed and vibration information. However, extracting target information using single-photon signal levels poses a critical challenge in extreme conditions. In this study, we propose a single-photon level FMCW lidar scheme. Quantum compressed sensing (QCS) is employed to simultaneously extract target distance and vibration information. Experimental results demonstrate successful synchronous detection at a beat frequency of 27.304 kHz and a vibration frequency of 500 Hz within an integration time of 0.125 s at a photon counting rate of 9 kcps. This approach provides a new, to the best of our knowledge, solution for FMCW radar application in extreme environments or long-range scenarios. © 2024 Optica Publishing Group. All rights, including for text and data mining (TDM), Artificial Intelligence (AI) training, and similar technologies, are reserved.

<https://doi.org/10.1364/AO.529686>

1. INTRODUCTION

Lidar is extensively employed in various industries, including defense, civil applications, and other fields, and has become an integral component of numerous equipment. In comparison with intensity measurement-based lidar techniques such as time-of-flight [1–6] and amplitude-modulated continuous wave, frequency-modulated continuous wave (FMCW) lidar utilizes coherent detection for acquiring target depth information, thereby exhibiting superior resistance against ambient light and stray light interference [7–12]. Simultaneously, by leveraging Doppler frequency shift information, it enables the synchronous extraction of target motion speed and vibration data [13–17], thus providing a more comprehensive dimension for data analysis.

However, in certain extreme environments such as long distances or foggy conditions, the detection terminal may only receive a limited number of photons [18–21]. The current single-photon lidar technology based on time-of-flight and photon counting has achieved remarkable advancements in imaging distance, reaching an astonishing 200 km [22]. Nevertheless, for FMCW lidar systems, which extract target distance and speed information through interference frequency analysis of signal and reference lights [23–26], traditional photon counting technology fails to meet the detection requirements due to its

prolonged integration time. In 2006, Luu *et al.* proposed to use single-photon detector array to improve the photon count rate to reduce the integration time, reconstruct the interference waveform through multiple measurements to reduce the shot noise, etc., and obtain the interference signal frequency through Fourier transform [27]. In 2008, Jiang *et al.* discussed in detail the optimal selection of local oscillator intensity, pointing out that single-photon detectors have very small electronic noise and can reach the limit of shot noise when the reference light is weak [28]. In 2013, Erkmen *et al.* proposed the maximum likelihood estimation method, using a single-photon detector to estimate the beat frequency of interference signals [29]. In the same year, Barber *et al.* discussed in detail the photon number and information efficiency required for FMCW laser ranging from the perspective of information theory [30]. In 2021, Chen *et al.* carried out sparse sampling through the traditional compressed sensing 1-bit quantization model to realize FMCW lidar based on single-photon detection [31,32]. From the above work, it can be seen that the study of single-photon FMCW lidar and its application is a trend in the future development of this field.

In this paper, we propose a FMCW single-photon ranging and vibration measurement system based on QCS, which enables simultaneous recovery of distance and vibrational frequency information of the target through discrete photon

detection. By leveraging the principle of QCS, our system constructs a compressed sensing framework utilizing the randomness inherent in coherent photon measurement collapse, thereby facilitating accurate recovery of broadband interference frequencies. The inherent uncertainty in quantum state measurement endows the measurement matrix in the compressed sensing algorithm with genuine randomness. In contrast with the pseudo-random matrix generated by conventional algorithms, this true randomness possesses a more universal nature, reducing our system's reliance on prior knowledge or assumptions regarding specific signal structures and thereby enhancing accuracy and robustness in signal reconstruction. Our experiments demonstrate the successful measurement of range and vibration information using single-photon FMCW lidar, thereby overcoming the limitations of traditional coherent detection in capturing single-photon beat frequency signals. This breakthrough technology holds great potential for applications in vehicle condition monitoring, bridge vibration testing, industrial production monitoring, and other extreme environments requiring precise range and vibration detection [33].

2. THEORY OF SINGLE-PHOTON FMCW LIDAR

The core principle of FMCW [11] lidar is to emit a laser beam with a continuously changing frequency, while receiving the reflected laser signal from the target object. The key to accurate measurement is to analyze the frequency difference between the transmitted signal and the received signal. In the time domain, the modulated signal is represented as a waveform diagram of the frequency density changing with time, as shown in Fig. 1(a). The spectral performance is shown in Fig. 1(b). In the time-frequency diagram, the frequency increases linearly with time, as shown in Fig. 1(c).

In this experiment, a Pound-Drever-Hall (PDH) laser frequency stabilization system was added at the light source. The system mainly measures the frequency of the laser through the Fabry–Perot cavity and feeds back the measured results to the laser to suppress the frequency fluctuation, which is an active feedback adjustment mode. In the actual measurement process, the system can generate error signals and actively feed back to the laser to realize the stable control of the laser output frequency. This effectively improves the time resolution, allowing the system to measure time delays or frequency changes more accurately. The light source for an FMCW lidar is a linear frequency modulated laser, which is then split into two beams by the beam splitter [34–37]. One beam serves as the signal light, while the other acts as the reference light. Upon reflection from the target, the outgoing signal light is received at the receiving

end and interferes with the reference light. Due to time delay experienced by the signal light during transmission, solving for beat frequency enables acquisition of distance information regarding the target

$$L = \frac{cT/n}{2B} f_b, \quad (1)$$

where L is the target distance, T is the frequency modulation period, B is the frequency modulation bandwidth, n is the medium refractive index, and f_b is the beat frequency. Ideally, the range resolution depends only on the modulation bandwidth

$$\Delta L = \frac{c/n}{2B}, \quad (2)$$

where the ideal beat signal frequency resolution $\Delta f_b = 1/T$. However, in the practical detection system, the spectral linewidth of the beat signal will be diffused during measurement due to laser phase noise and frequency modulation nonlinearity. The range resolution ΔL is determined by the modulation bandwidth and the spectral linewidth of the beat signal:

$$\Delta L = \frac{cT/n}{2B} \Delta f_b, \quad \Delta f_b > \frac{1}{T}. \quad (3)$$

For a target with vibration characteristics, its velocity component in the direction of optical transmission will cause the signal light to produce a Doppler shift, resulting in a change in the phase of the reflected light. After the interference of the reflected light and reference light, the phase difference between the two beams can be obtained, and the vibration frequency information of the target can be extracted accordingly.

Under classical optical conditions, the optical field is in a coherent state, and frequency modulated continuous wave (FMCW) lidar utilizes the interference effect of the optical field to recover target distance and vibration information. Interference is a manifestation of the wave nature of light, describing the relationship between the phases of light waves. By analyzing the position of interference fringes or the variation of interference signals, distance information of the target can be extracted. Typically, classical electromagnetic theory can be used to describe the propagation of the optical field and interference phenomena. However, under extreme conditions such as long distances or heavy fog, the receiver can only receive a small amount of discrete photon signals. It cannot be simply assumed that the photons are in a coherent state. It is necessary to consider the wave and particle properties of photons. This means that not only the interference effect of photons must be taken into account but also the time and position of individual

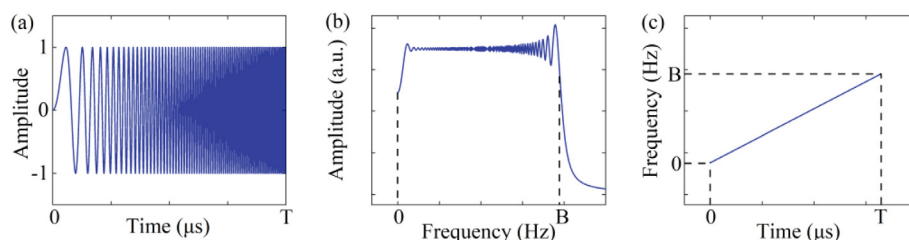


Fig. 1. Linear frequency modulation signal.

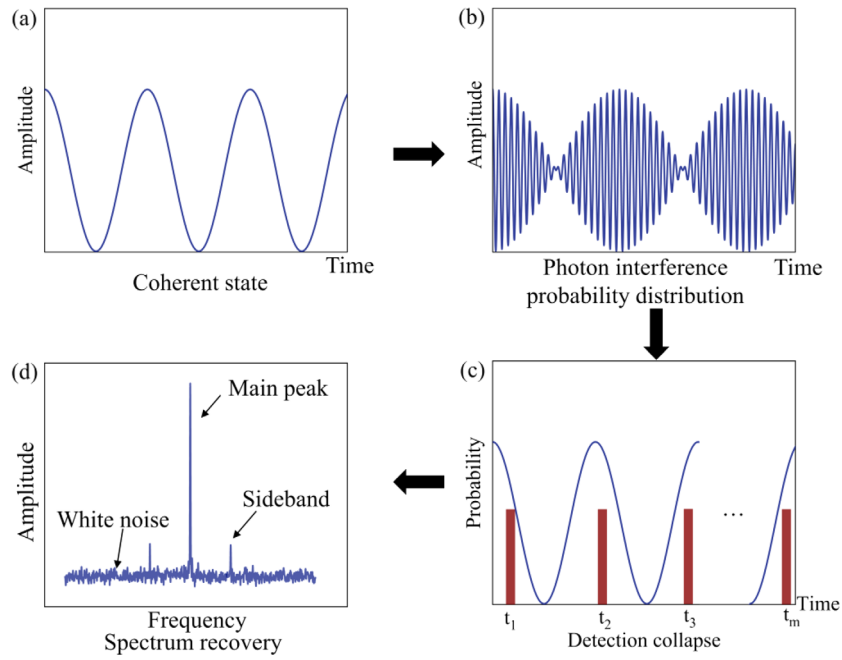


Fig. 2. QCS sampling and signal reconstruction, where (a), (b), (c) are the schematic diagrams, and (d) is the experimental result. (a) Initial quantum state $|\alpha\rangle$, which is a coherent state in this work. (b) Map of sparse signal x to be measured to the initial quantum state. In the experiment, the time-varying signal x is mapped to the coherent state $|\alpha\rangle$ using a Mach–Zehnder intensity modulator, the output quantum state is expressed as $|\alpha^x\rangle$. (c) When the photon is detected in the time domain at the level of single photon, it will randomly collapse to a certain time, and the probability of measuring the collapse is directly related to the waveform, $y' = \hat{A}|\alpha^x\rangle$. (d) Spectral reconstruction is achieved by performing discrete Fourier transform on photon arrival times.

photon arrivals. By accumulating the counting information of single photons, we can reconstruct the distance information of the target. In this case, quantum optics theory must be employed to describe the behavior of the optical field and photons. Consequently, extracting target information from these discrete signals poses a primary challenge to be addressed. Due to the sparsity of the beat signal in the frequency domain, signal compression measurement can be achieved for sparse signals in the transformed domain, based on the principle of compressed sensing.

Here, QCS can be defined as a signal processing technique for efficiently acquiring and reconstructing signals from considerably fewer samples than required by the Nyquist–Shannon theorem by constructing a compressive measurement system using quantum resources, such as quantum coherence, quantum entanglement, etc. In this paper, the QCS method is used to sample and reconstruct the beat signal. The information extraction process is shown in Fig. 2. Its mathematical model can be expressed as $y' = \hat{A}|\alpha^x\rangle$, where $|\alpha\rangle$ is the initial quantum state, as shown in Fig. 2(a). Map the sparse signal x to be measured to the initial quantum state to ensure that the measured collapse probability distribution is consistent with the signal, and the output quantum state is expressed as $|\alpha^x\rangle$, as shown in Fig. 2(b). \hat{A} denotes the observation operator, and y' denotes the measurement result. The measurement operator of QCS does not directly determine the measurement matrix, which is formed only when the measurement occurs due to the random collapse of the quantum state $|\alpha^x\rangle$. Since $|\alpha^x\rangle$ is directly related to the measured signal x , the measurement matrix is determined

by the initial state $|\alpha^x\rangle$, the measured signal x , and the measurement operator \hat{A} . The next step is to collect the arrival time of the detected photon, as shown in Fig. 2(c). This is different from the time and amplitude information required for traditional sampling, because the signal output by the single photon detector is a standard pulse signal, which only represents the arrival time of the photon and does not contain the intensity information. Thus, assuming the amplitude of each pulse is one, the horizontal axis corresponds to the collapse time of the photon. In this work, the detected signal (i.e., $|\alpha^x\rangle$) consists of the beat frequency signal between the probe light and the reference light. Respectively, we collect the $|e_i, 0\rangle$ and $|e_j, 0\rangle$ for the i direction and j direction eigen state of two orthogonal vectors. Since there is a time delay between the probe light and the reference light, the corresponding phase difference φ will be generated. The quantum expression of the beat signal is expressed as [38]

$$\hat{P}_{\text{beat}} = [1 + \exp(i\varphi)] \times (|e_i, 0\rangle\langle e_i, 0| + |e_j, 0\rangle\langle e_j, 0|). \quad (4)$$

Therefore, the beat signal is only determined by the phase difference, and because the laser phase is linearly modulated, the probability of the photon being detected varies periodically.

Mathematically, a coherent state is defined to be the eigenstate of the annihilation operator \hat{a} with corresponding eigenvalue α , that is, $\hat{a}|\alpha\rangle = \alpha|\alpha\rangle$, where $\alpha = |\alpha|e^{i\psi}$, $|\alpha|$ and ψ are called the amplitude and phase of the state $|\alpha\rangle$. Similarly, the detection of manipulated quantum state $|\alpha^x\rangle$ could also be expressed as

$$y' = \hat{a}|\alpha^x\rangle = \frac{x(t)}{\max(x(t))} \alpha e^{i\psi}, \quad (5)$$

since direct photon detection cannot reflect phase information, without loss of generality, we can assume that $\psi = 0$. Equation (5) shows that the probability of photon detection is proportional to the signal $x_{(t)}$. The result of the quantum state detection is a vector $y' = \{y_1, y_2, \dots, y_m, \dots, y_M, M \ll N\}$ of length M (suppose x is a 1D discrete-time signal with length N), representing the photon arrival time-series.

For signal recovery, the time domain signals of random arrival of photons are collected by a single-photon detector and time interval analyzer. In this work, the single photon beat signal is converted to the frequency domain by DFT, and the target distance is solved by locating the main peak position of the spectrum, as shown in Fig. 2(d). By solving the relative position difference between the main peak and the first-order sideband, the vibration frequency of the target can be obtained.

The essential differences between classical and quantum detection are whether the properties of quantum physics are exploited and whether quantum advantages are demonstrated. In our work, the construction of the quantum compressed sensing system is based on the randomness of the coherent state measurement collapse, which is a fundamental property of quantum physics and the basis of the widely studied quantum random numbers. The classical compressed sensing observation matrix is constructed by using artificially constructed pseudorandom numbers, and sub-Nyquist sampling of measured signals is carried out by an analog-to-digital conversion module. In this work, the measured signal is a beat signal, but because the received light intensity is sparse photon signal, its waveform cannot be detected by analog-to-digital conversion module, so the classical compressed sensing cannot work. The method proposed in this paper uses sparse photon detection directly to extract beat frequency information, which is also an embodiment of the advantage of quantum measurement.

3. EXPERIMENTAL SYSTEM AND RESULT ANALYSIS

The experimental setup diagram of this study is illustrated in Fig. 3. We used a narrow linewidth external cavity tunable laser with a wavelength of 1550 nm as our light source. The free line width of the laser is about 100 kHz. To ensure laser frequency stability, we employ the PDH frequency-locking technique to achieve linewidth compression of the laser frequency. After compression, the laser linewidth reaches 13 Hz [39].

First, the laser output is split into two parts using an optical fiber splitter. One part of the light is directed into a hyperstable cavity for frequency stabilization. After the output passes through the hyperstable cavity, one end is transmitted to Photoelectric Detector 2 (PD 2) for real-time frequency monitoring, while the other end is transmitted to Photoelectric Detector 1 (PD 1). The light received by the PD 1 is then transferred to an electrical mixer, and, after mixing with the reference frequency provided by a function signal generator (Tektronix, AFG3102) from the hyperstable cavity, it is transmitted to a proportional integral derivative (PID) circuit for frequency error calculation. Subsequently, the error signal is fed back to the laser through the main output port of the PID, which is inputted into the laser's direct current port to achieve higher bandwidth noise feedback control. Additionally, the error signal from the auxiliary output port of the PID is transmitted to the piezoelectric ceramic end of the laser to compensate for frequency drift caused by long-term laser transmission.

An electro-optic modulator (EOM) is utilized for loading a linear frequency modulation signal. The EOM receives a sawtooth waveform modulated radio-frequency (RF) signal from an RF signal generator (Stanford Research Systems, Inc. Model SG386), which is further amplified by an electrical gain module (Mini-Circuits, ZVA-183 G-S+) to achieve linearly modulated laser output. After the modulated laser beam is split by a fiber beam splitter (BS), one portion is utilized as the signal beam, while the other serves as the reference beam. The signal light is collimated through a collimator head, with a mirror serving as the target. The lens group collects and polarizes the reflected light generated by the target before transmitting it to

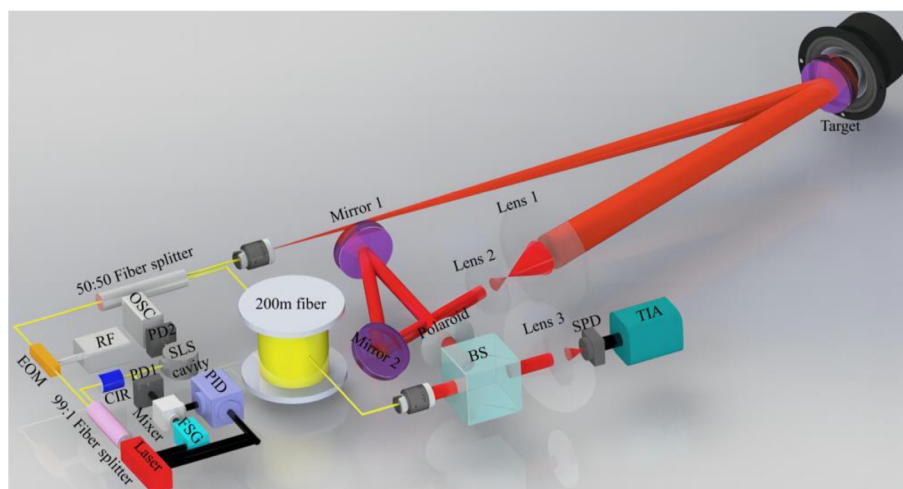


Fig. 3. Experimental setup. CIR, circulator; PD, photoelectric detector; FSG, function signal generator; RF, radio frequency signal generator; EOM, electro-optic modulator; BS, 50:50 beam splitter; SPD, single-photon detector; TIA, time interval analyzer; OSC, oscilloscope.

free space BS. Following its passage through a 200 m delayed optical fiber, the reference light is attenuated to a level close to the detection light intensity using an optical attenuator (Thor Labs, VOA50-APC) and adjusting polarization. Due to the low sweep rate of the radio-frequency source driven EOM, a 200 m delay fiber was added in the experiment, which increased the time delay between the reference light and the signal light by about 1 μ s. Then, it is emitted into free space and interferes with the detection beam at the beam splitter (BS).

In order to validate the accuracy of the system, we employ classical and quantum detection techniques to compare the interference signal detection outcomes. Initially, the interference beam is detected using a photodetector (Thorlabs, APD430C/M), followed by collection of time domain signals through an oscilloscope (LeCroy Wave Surfer 44MXs-B). Subsequently, computer postprocessing software performs a discrete Fourier transform (DFT) analysis. The target distance and vibration information are obtained by analyzing the spectrum. For single-photon detection, a dedicated single-photon detector (ID230) is employed to capture photons, while their arrival time is recorded using a high-precision time interval analyzer (TIA, SIMINICS, FT1040). Subsequently, computer postprocessing techniques are applied to determine the distance and vibration information of the target using the QCS algorithm.

In theory, the range resolution is solely determined by the frequency modulation bandwidth. However, in practical application scenarios, the propagation of laser over long distances introduces phase noise, thereby increasing the full width at half maximum (FWHM) of the beat frequency spectrum, as depicted in Fig. 4(a). In this experiment, the utilization of PDH frequency locking technology effectively mitigates phase noise, resulting in a significant reduction of the FWHM of the beat frequency spectrum and an enhanced distance resolution. As depicted in Fig. 4(b), the FWHM of the spectrum is reduced

from 63 to 8.15 Hz. Figures 4(c) and 4(d) illustrate spectrum obtained during vibration testing without and with frequency locking, respectively.

A. Classical FMCW Vibration Measurement

In the experiment, a reflector was used as the target object for distance and vibration testing, as shown in Fig. 5. The distance difference between the reference end and the detection end was set to be approximately 103.4 m, employing a linear frequency modulation signal featuring a center frequency of 4.5 GHz and modulation bandwidth of 3.3 GHz. A linear modulation signal with a modulation period of 0.125 s was applied to modulate the output laser frequency. The oscilloscope sampling rate was set to 200 kS/s [the measurement results are shown in Fig. 5(a); further, when the target is stationary, the beat signal exhibits a center frequency of 27.304 kHz. At this juncture, Gaussian fitting of the measured beat frequency spectrum yields an FWHM value of 12.67 Hz, corresponding to a ranging resolution of 4.79 cm. In the vibration measurement, a loudspeaker is positioned behind the target to regulate the vibration amplitude and frequency by connecting the signal input of the loudspeaker to a function signal generator. Figure 5(b) shows the vibration test spectrum diagram of the loudspeaker when the vibration frequency is 100 Hz and the driving voltage is 100 mV (red line in the figure), 400 mV (yellow line in the figure), and 500 mV (blue line in the figure). Figure 5(c) shows the vibration test spectrum diagram of the loudspeaker when the vibration frequency is 500 Hz and the driving voltage is 500 mV. It can be observed that sidebands with frequency intervals of f_v are present around the center frequency. It can be concluded that the distance and vibration frequency of the target can be extracted from the positions of the spectral peaks and sidebands in the spectrum. The

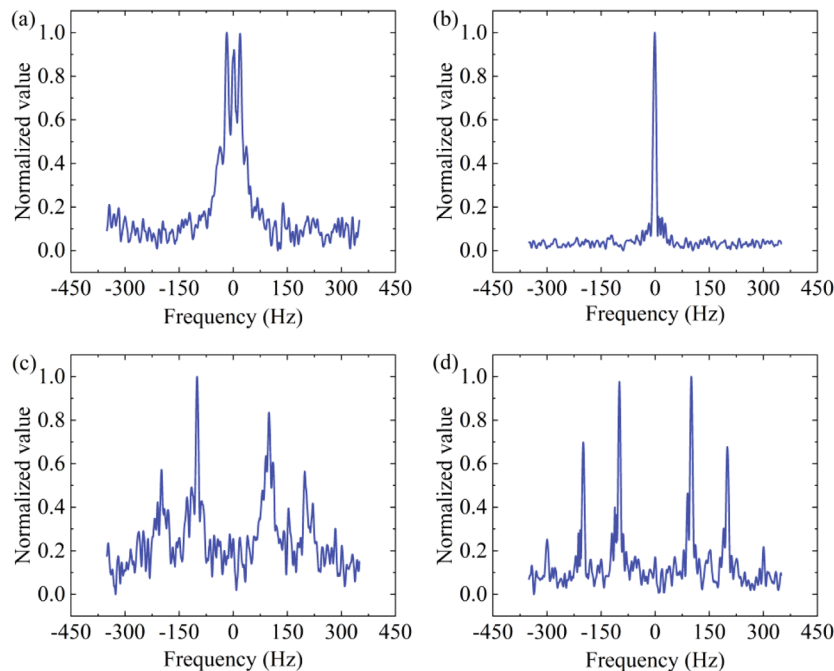


Fig. 4. (a) Spectrum of interference signal without frequency locking. (b) Spectrum of interference signal with frequency locking. (c) Vibration spectrum without frequency locking. (d) Vibration spectrum with frequency locking.

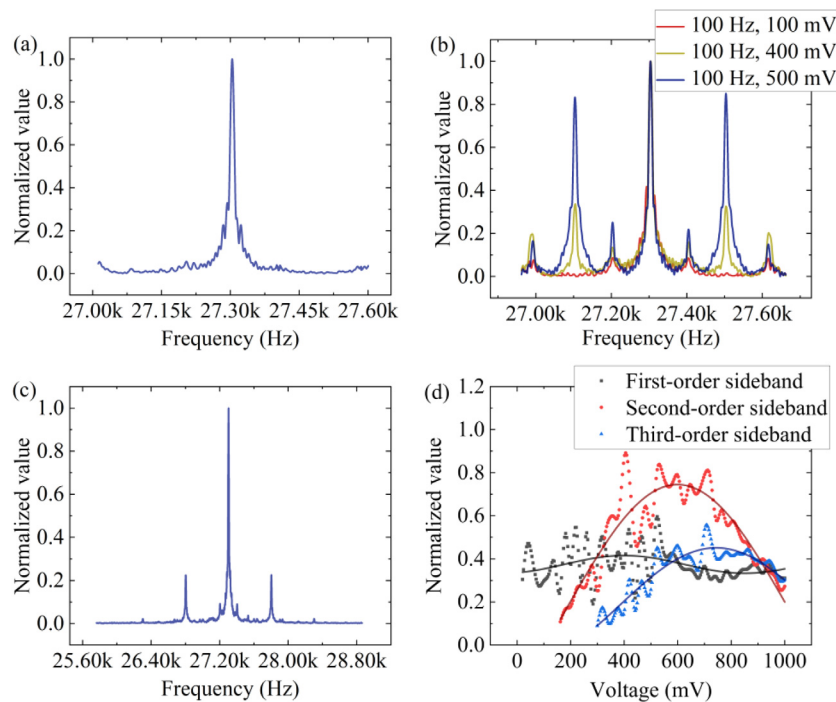


Fig. 5. Interference spectrum of FMCW with classical photodetector. (a) Spectrum diagram of stationary target interference signal. (b) Vibration test spectrum diagram of loudspeaker with vibration frequency of 100 Hz, driving voltage of 100 mV (red line in figure), 400 mV (yellow line in figure), and 500 mV (blue line in figure). (c) Loudspeaker vibration frequency is 500 Hz, driving voltage is 500 mV spectrum diagram. (b) and (c) are collected when the sampling rate of oscilloscope is 200 kS/s. (d) Variation trend of normalized sideband amplitude.

variation in sideband intensity is closely related to the amplitude of the target's vibration. To determine the relationship between sideband intensity and target amplitude variation, experiments were conducted. The results shown in Fig. 5(d) describe the trend of each order sideband as the speaker's drive voltage continues to increase from 20 to 1000 mV while keeping the vibration frequency fixed at 100 Hz. As the vibration amplitude of the target increases, the amplitude of the sideband also increases, and when the amplitude of the vibration exceeds one wavelength cycle (that is, 1550 nm), a second-order sideband is generated and gradually becomes stronger. As the amplitude continues to increase, the third-order sideband also has the same trend. At the same time, due to the energy transfer between the sideband, the amplitude of the high-order sideband increases, while the amplitude of the low-order sideband decreases. Figure 5(b) shows a fixed-noise signal around 300 Hz, which is caused by residual amplitude modulation due to PDH locking.

B. Vibration Measurement by Single-Photon FMCW Lidar

In the experiment of single-photon FMCW lidar range and vibration measurement, the target distance is set to 103.4 m. An adjustable fiber attenuator is introduced into the optical path to artificially attenuate the signal light and reference light to a single photon level. The detector is replaced by a single-photon detector (ID230). The time-series of photon arrival is recorded by time interval analyzer. Here, we set the photon counting rate to 9 kcps, with a dead time of 2 μ s for the single-photon detector and approximately 300 cps for dark counts. The time

interval analyzer's time resolution is set to 16 ps. By applying the quantum compressive sensing algorithm to reconstruct the signal from discrete photons in the sparse domain, we can obtain an interference spectrum containing target distance and vibration information at the single-photon level. The measurement results obtained under the same experimental conditions are shown in Fig. 6. Gaussian fitting of the measured ranging beat frequency spectrum shown in Fig. 6(a) yields a spectrum FWHM of 8.15 Hz, corresponding to a distance resolution of 3.08 cm. In Figs. 6(b) and 6(c), we used the same experimental parameters as in Figs. 5(b) and 5(c) for spectrum recovery under the single-photon condition. We kept the same measurement settings and experimental conditions for comparison. By comparing with the classical test results in Figs. 5(b) and 5(c), it can be concluded that the system can achieve distance and vibration measurements within 0.125 s integration time using a photon counting rate of 9 kcps, meeting the requirements for distance and vibration measurement under extremely weak signal light conditions. In addition, the trend of sideband and amplitude variation at the single-photon level is experimentally verified, as shown in Fig. 6(d). The trend of sideband variation is consistent with the trend of sideband variation under classical optical conditions, which verifies the reliability of measurement results of the experimental system. Our method extracts the target signal at the level of single photon, and, when the number of photons is low, it is inevitably affected by quantum shot noise. Shot noise is inherent in the method and cannot be eliminated. It appears as white noise in the frequency domain, which will cause interference to the spectrum signal-to-noise ratio, which makes it

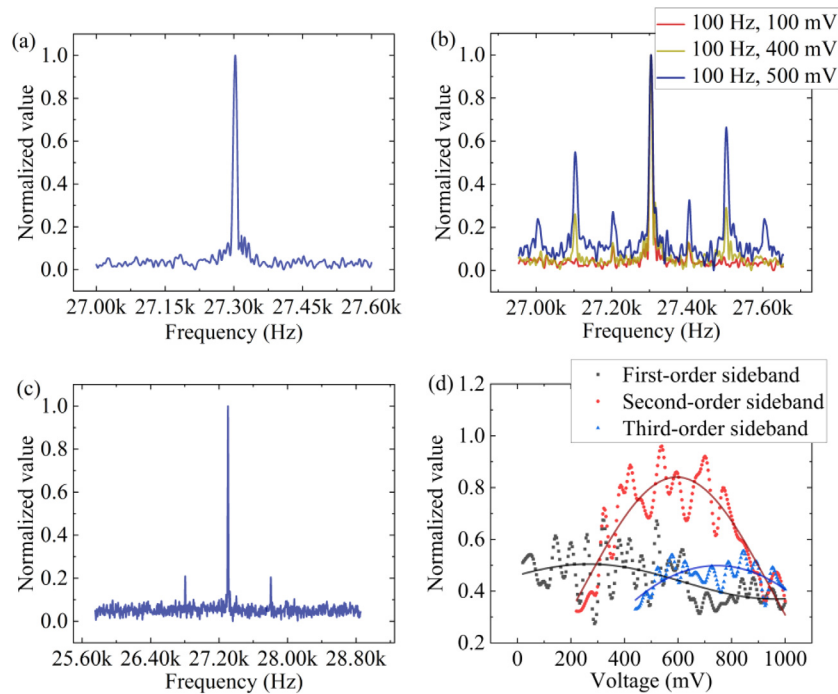


Fig. 6. Spectrum of distance and vibration measurement at the single-photon level. (a) Interference spectrum diagram of stationary object. (b) Vibration test spectrum diagram of loudspeaker with vibration frequency of 100 Hz, driving voltage of 100 mV (red line in figure), 400 mV (yellow line in figure), and 500 mV (blue line in figure). (c) Loudspeaker vibration frequency is 500 Hz, driving voltage is 500 mV spectrum diagram. (d) Single-photon order normalized sideband amplitude variation trend.

impossible for the proposed method to reduce the photon count rate without limitation.

4. CONCLUSION

The present work proposes a compound FMCW system for single-photon ranging and vibration measurement system based on the QCS. Our approach addresses the limitation of traditional coherent detection in measuring single-photon beat frequency signals. By detecting discrete photons, both distance and vibration information of remote targets can be simultaneously retrieved. The experiment demonstrates the measurement of range and vibration information of single-photon FMCW lidar, which fulfills the requirements for range and vibration detection in extreme environments. The experimental results indicate that, under a photon count rate of 9 kcps, synchronous detection of beat frequency 27.304 kHz and vibration frequency 500 Hz can be achieved with an integration time of only 0.125 s. The photon-level FMCW lidar provides us with a new mode of lidar operation, which can realize a longer detection distance and take into account the functions of ranging, velocity measurement, vibration measurement, and so on. Next, we will focus on further distance, strong background environment photon-level FMCW research. This work is of great significance for extreme environment, vehicle radar, and military reconnaissance. Moreover, it holds potential applications in noninvasive heart detection, muscle behavior assessment, bone vibration analysis, etc., offering novel perspectives for diagnosing and treating cardiovascular diseases.

Funding. National Natural Science Foundation of China (62075120, 62075122, 62105193, 62127817, 62205187, 62222509, 62305200, U22A2091); Shanxi Province Science and Technology Major Special Project (202201010101005); National Key Research and Development Program of China (2022YFA1404201); Program for Changjiang Scholars and Innovative Research Team in University (IRT_17R70); China Postdoctoral Science Foundation (2022M722006); Shanxi Province Science and Technology Innovation Talent Team (202204051001014); Science and Technology Cooperation Project of Shanxi Province (202104041101021); Shanxi “1331 Project”; 111 Project (D18001).

Disclosures. The authors declare no conflicts of interest.

Data availability. Data underlying the results presented in this paper are not publicly available at this time but may be obtained from the authors upon reasonable request.

REFERENCES

1. M.-C. Amann, T. Bosch, M. Lescure, *et al.*, “Laser ranging: a critical review of usual techniques for distance measurement,” *Opt. Eng.* **40**, 10–19 (2001).
2. G. Berkovic and E. Shafir, “Optical methods for distance and displacement measurements,” *Adv. Opt. Photon.* **4**, 441–471 (2012).
3. G. Salata, L. R. Cenkeramaddi, V. K. Huynh, *et al.*, “Time–frequency analysis and fault prediction of motor bearings using millimeter-wave radar,” *IEEE Sens. J.* **23**, 18718–18728 (2023).
4. D. Goyal and B. S. Pabla, “The vibration monitoring methods and signal processing techniques for structural health monitoring: a review,” *Arch. Comput. Methods Eng.* **23**, 585–594 (2015).
5. S. Li, Y. Xiong, X. Shen, *et al.*, “Multi-scale and full-field vibration measurement via millimetre-wave sensing,” *Mech. Syst. Signal Process.* **177**, 109178 (2022).
6. S. Jiang, D. Sun, Y. Han, *et al.*, “Performance of continuous-wave coherent Doppler lidar for wind measurement,” *Curr. Opt. Photon.* **3**, 466–472 (2019).

7. W. Jiang, M. Fujigaki, Y. Uchida, *et al.*, "Measurement of out-of-plane displacement in time series using laser lines and a camera with a diffraction grating," *Opt. Laser Eng.* **151**, 106891 (2022).
8. T. Anna, C. Shakher, D. S. Mehta, *et al.*, "Three-dimensional shape measurement of micro-lens arrays using full-field swept-source optical coherence tomography," *Opt. Laser Eng.* **48**, 1145–1151 (2010).
9. K. Kou, C. Wang, and Y. Liu, "All-phase FFT based distance measurement in laser self-mixing interferometry," *Opt. Laser Eng.* **142**, 106611 (2021).
10. D. Uttam and B. Culshaw, "Precision time domain reflectometry in optical fiber systems using a frequency modulated continuous wave ranging technique," *J. Lightwave Technol.* **3**, 971–977 (1985).
11. J. Zheng, "Optical frequency-modulated continuous-wave interferometers," *Appl. Opt.* **45**, 2723–2730 (2006).
12. Y. Wang, "Frequency-swept feedback interferometry for noncooperative-target ranging with a stand-off distance of several hundred meters," *Photonix* **3**, 21 (2022).
13. Y. Xiong, Z. Peng, G. Xing, *et al.*, "Accurate and robust displacement measurement for FMCW radar vibration monitoring," *IEEE Sens. J.* **18**, 1131–1139 (2018).
14. L. Wampler, F. Xia, S. Y. F. Yeung, *et al.*, "A Doppler radar with a sweeping lock-in demodulator for machine vibration sensing," *IEEE Sens. J.* **23**, 28833–28844 (2023).
15. Z. Zang, X. Yang, G. Zhang, *et al.*, "Video-based vibration measurement using an unmanned aerial vehicle: an anti-disturbance algorithm for the shaking of airborne cameras," *IEEE Trans. Instrum. Meas.* **72**, 5024116 (2023).
16. P. O'Donoghue, F. Gautier, E. Meteyer, *et al.*, "Comparison of three full-field optical measurement techniques applied to vibration analysis," *Sci. Rep.* **13**, 3261 (2023).
17. L. Ding, M. Ali, S. Patole, *et al.*, "Vibration parameter estimation using FMCW radar," in *IEEE International Conference on Acoustics, Speech and Signal Processing (ICASSP)* (2016), pp. 2224–2228.
18. W. Maddern, G. Pascoe, C. Linegar, *et al.*, "1 year, 1000 km: the Oxford RobotCar dataset," *Int. J. Robot. Res.* **36**, 3–15 (2016).
19. F. Zappa, S. Tisa, A. Tosi, *et al.*, "Principles and features of single-photon avalanche diode arrays," *Sens. Actuators A, Phys.* **140**, 103–112 (2007).
20. G. A. Shaw, A. M. Siegel, J. Model, *et al.*, "Deep UV photon-counting detectors and applications," *Proc. SPIE* **7320**, 73200J (2009).
21. G. A. Howland, P. B. Dixon, and J. C. Howell, "Photon-counting compressive sensing laser radar for 3D imaging," *Appl. Opt.* **50**, 5917–5920 (2011).
22. Z.-P. Li, J.-T. Ye, X. Huang, *et al.*, "Single-photon imaging over 200 km," *Optica* **8**, 344–349 (2021).
23. Y. Li, S. Verstyuyft, G. Yurtsever, *et al.*, "Heterodyne laser Doppler vibrometers integrated on silicon-on-insulator based on serrodyne thermo-optic frequency shifters," *Appl. Opt.* **52**, 2145–2152 (2013).
24. S. Suyama, H. Ito, R. Kurahashi, *et al.*, "Doppler velocimeter and vibrometer FMCW LiDAR with Si photonic crystal beam scanner," *Opt. Express* **29**, 30727–30734 (2021).
25. G. F. Alfrey, "The laser Doppler technique," *Phys. Bull.* **31**, 319 (1980).
26. P. Trocha, J. N. Kemal, Q. Gaimard, *et al.*, "Ultra-fast optical ranging using quantum-dash mode-locked laser diodes," *Sci. Rep.* **12**, 1076 (2022).
27. J. X. Luu and L. A. Jiang, "Saturation effects in heterodyne detection with Geiger-mode InGaAs avalanche photodiode detector arrays," *Appl. Opt.* **45**, 3798–3804 (2006).
28. L. A. Jiang and J. X. Luu, "Heterodyne detection with a weak local oscillator," *Appl. Opt.* **47**, 1486–1503 (2008).
29. B. I. Erkmen, Z. W. Barber, and J. Dahl, "Maximum-likelihood estimation for frequency-modulated continuous-wave laser ranging using photon-counting detectors," *Appl. Opt.* **52**, 2008–2018 (2013).
30. Z. W. Barber, J. R. Dahl, T. L. Sharpe, *et al.*, "Shot noise statistics and information theory of sensitivity limits in frequency-modulated continuous-wave radar," *J. Opt. Soc. Am. A* **30**, 1335–1341 (2013).
31. Z. Chen, B. Liu, G. Guo, *et al.*, "Photon counting heterodyne with a single photon avalanche diode," *IEEE Photon. Technol. Lett.* **33**, 931–934 (2021).
32. B. Du, C. Pang, D. Wu, *et al.*, "High-speed photon-counting laser ranging for broad range of distances," *Sci. Rep.* **8**, 4198 (2018).
33. H. Jang, J. W. Kim, G. H. Kim, *et al.*, "Simultaneous distance and vibration mapping of FMCW-LiDAR with a kinetic external cavity diode laser," *Opt. Laser Eng.* **160**, 107283 (2023).
34. H. Lee, G. H. Kim, M. Villiger, *et al.*, "Linear-in-wavenumber actively-mode-locked wavelength-swept laser," *Opt. Lett.* **45**, 5327–5330 (2020).
35. J. Riemensberger, A. Lukashchuk, M. Karpov, *et al.*, "Massively parallel coherent laser ranging using a soliton microcomb," *Nature* **581**, 164–170 (2020).
36. A. Martin, D. Dodane, L. Leviandier, *et al.*, "Photonic integrated circuit-based FMCW coherent LiDAR," *J. Lightwave Technol.* **36**, 4640–4645 (2018).
37. C. Zhang, T. Nagata, M. S. B. A. Sharifuddin, *et al.*, "Long-range frequency-modulated continuous-wave LiDAR employing wavelength-swept optical frequency comb," *Opt. Commun.* **545**, 129702 (2023).
38. C. Holbrow, E. Galvez, M. E. Parks, *et al.*, "Photon quantum mechanics and beam splitters," *Am. J. Phys.* **70**, 260–265 (2002).
39. M. Jing, P. Zhang, S. Yuan, *et al.*, "High bandwidth laser frequency locking for wideband noise suppression," *Opt. Express* **29**, 7916–7924 (2021).